***J. Ocean Univ. China*** (Oceanic and Coastal Sea Research)
DOI 10.1007/s11802-014-2060-4
ISSN 1672-5182, 2014 13 (4): 561-571
*http://www.ouc.edu.cn/xbywb/*
*E-mail:xbywb@ouc.edu.cn*

# Modeling Seasonal Variations of Subsurface Chlorophyll Maximum in South China Sea

GONG Xiang, SHI Jie, and GAO Huiwang*

*Key Laboratory of Marine Environment and Ecology*, *Ocean University of China*, *Qingdao* 266100, *P. R. China*

(Received May 28, 2012; revised June 11, 2012; accepted March 13, 2014)


**Abstract** In the South China Sea (SCS), the subsurface chlorophyll maximum (SCM) is frequently observed while the mechanisms of SCM occurrence have not been well understood. In this study, a 1-D physical-biochemical coupled model was used to study the seasonal variations of vertical profiles of chlorophyll-*a* (Chl-*a*) in the SCS. Three parameters (*i.e.*, SCM layer (SCML) depth, thickness, and intensity) were defined to characterize the vertical distribution of Chl-*a* in SCML and were obtained by fitting the vertical profile of Chl-*a* in the subsurface layer using a Gaussian function. The seasonal variations of SCMs are reproduced reasonably well compared to the observations. The annual averages of SCML depth, thickness, and intensity are 75±10 m, 31±6.7 m, and 0.37±0.11 mg $m^{-3}$, respectively. A thick, close to surface SCML together with a higher intensity occurs during the northeastern monsoon. Both the SCML thickness and intensity are sensitive to the changes of surface wind speed in winter and summer, but the surface wind speed exerts a minor influence on the SCML depth; for example, double strengthening of the southwestern monsoon in summer can lead to the thickening of SCML by 46%, the intensity decreasing by 30%, and the shoaling by 6%. This is because part of nutrients are pumped from the upper nutricline to the surface mixed layer by strong vertical mixing. Increasing initial nutrient concentrations by two times will increase the intensity of SCML by over 80% in winter and spring. The sensitivity analysis indicates that light attenuation is critical to the three parameters of SCM. Decreasing background light attenuation by 20% extends the euphotic zone, makes SCML deeper (~20%) and thicker (12%–41%), and increases the intensity by over 16%. Overall, the depth of SCML is mainly controlled by light attenuation, and the SCML thickness and intensity are closely associated with wind and initial nitrate concentration in the SCS.

**Key words** South China Sea; subsurface chlorophyll maximum; seasonal variation; numerical modeling

## 1 Introduction

Subsurface chlorophyll (Chl-*a*) maximums (SCMs) commonly occur in world's oceans (Cullen, 1982; Holm-Hansen and Hewes, 2004; Martin *et al.*, 2010; Venrick, 1993), especially throughout much of the tropical and subtropical oceans (Cullen, 1982; Radenac and Rodier, 1996; Teira *et al.*, 2005). Seasonal SCMs are frequently developed in temperate latitudes (Hopkinson and Barbeau, 2008; Venrick, 1993), and even in arctic and subarctic latitudes (Holm-Hansen and Hewes, 2004; Martin *et al.*, 2010). The biomasses in the SCM layer (SCML) make a significant contribution to primary production in the whole water column (Hanson *et al.*, 2007; Siswanto *et al.*, 2005; Weston *et al.*, 2005). Pérez *et al.* (2006) showed that 65%–75% of the total chlorophyll in a water column of the Atlantic subtropical gyres is present in SCML. The SCML accounts for 58% of water column primary production in the central North Sea (Weston *et al.*, 2005).

* Corresponding author. Tel: 0086-532-66782977
E-mail: hwgao@ouc.edu.cn

Since Riley *et al.* (1949) first found the SCMs in the western North Atlantic, the mechanisms leading to SCMs have been investigated. Based on previous studies, a common explanation can be: 1) There exists a nutrient-poor surface layer due to rapid phytoplankton consumption; 2) Phytoplankton either undergo an active migration (Klausmeier and Litchman, 2001) to or sink into subsurface layer (Hodges and Rudnick, 2004; Huisman *et al.*, 2006; Jamart *et al.*, 1977); 3) In subsurface layer the Photosynthetic Available Radiation (PAR) is not a limitation factor and rich nutrients satisfy the phytoplankton growth. Some studies proposed that in oligotrophic ocean SCMs may result from increased chlorophyll content of phytoplankton with depth at low light levels (*i.e.*, photoacclimation of phytoplankton in the euphotic zone) (Cullen, 1982; Fennel and Boss, 2003).

SCMs can be characterized using three parameters, *i.e.*, depth, thickness, and intensity of the SCML. Various studies explored the variability of the three parameters in different oceans (Pérez *et al.*, 2006; Radenac and Rodier, 1996; Teira *et al.*, 2005). Generally, the three parameters are respectively deeper, thicker and smaller in open oceans than in coastal seas (Gong *et al.*, 2012). The SCML in

tropical and subtropical oceans evidently deepens from winter to summer (Hense and Beckmann, 2008; Teira *et al.*, 2005). The thickness and intensity of SCML vary significantly from one month to another in the Pacific Ocean (Hense and Beckmann, 2008). In the Eastern North Atlantic Subtropical Gyre, the SCML intensity almost remains constant year around (Teira *et al.*, 2005). However, questions such as what causes the seasonal variation of the three parameters remain to be answered.

The South China Sea (SCS) (Fig.1) is the largest marginal sea along china's coasts and has an area of more than $3.5\times10^6$ km$^2$ with the maximum depth greater than 5000 m. The SCS is located within the East Asia monsoon region. The northeastern monsoon prevails from late September to April, whereas the southwestern monsoon prevails from May to early September (Shaw *et al.*, 1996). It is conceivable that the biogeochemistry of the SCS could respond to the alternating monsoons. For example, a winter phytoplankton bloom off the northwest Luzon is well associated with an increase of ambient nutrients due to the upwelling under the northeastern monsoon (Chen *et al.*, 2006; Tang *et al.*, 1999).

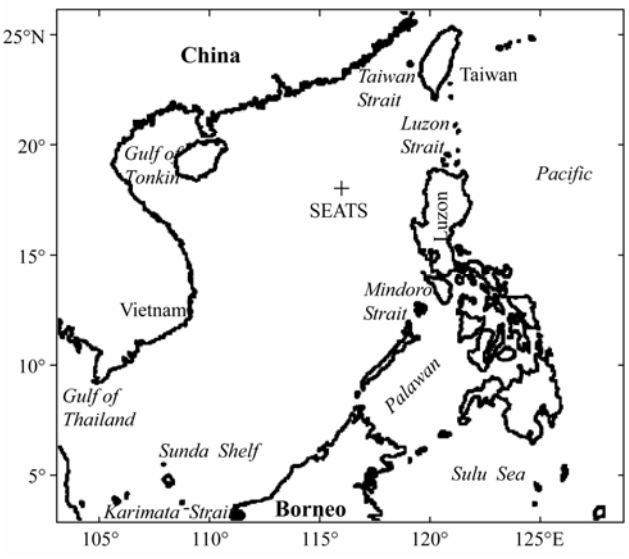


Fig.1 The SCS and the South East Asian Time-series Study (SEATS) station.

To understand biogeochemical responses to monsoon and other physical forcing (*e.g.*, typhoons, internal waves, circulations, *etc.*) in the SCS, the South East Asia Time-series Study (SEATS, Fig.1) was initiated in 1999. The SEATS station is located at about 18˚N and 116˚E and has a water depth of about 3800 m. Within the JGOFS (Joint Global Ocean Flux Study) program SEATS is a unique time-series study on marginal seas. The first data survey was carried out from September 1999 to July 2000, and afterwards about four times per year. Wong *et al.* (2007a) reviewed the data obtained primarily between 1999 and 2003. They concluded that in contrast to the generally accepted notion that seasonal variations in the tropical waters are minimal, well defined and regular seasonal patterns were observed in the carbon cycle, the nutrient dynamics and the biological community structure in the northern SCS. However, the study of SCMs in the SCS is limited. Liu *et al.* (2007) suggested that the photo-adaptation of phytoplankton can be critical to the development of SCMs in the SCS. Lu *et al.* (2010) found that the variable SCML depth and intensity are controlled by the upwelling, river plume, and associated biological balances among light, nutrients and planktons in the northern SCS in summer. Chen *et al.* (2006) reported that the seasonal variations of SCML depth and intensity at 19˚N and 118.5˚E are within the winter upwelling zone centered at about 100 km northwest off Luzon in the SCS.

In this study, a process-oriented 1-D model was used to simulate the seasonal variations and to understand the controlling mechanisms of SCMs in the SCS. Building on the model results, a Gaussian function was used to fit the vertical profile of Chl-*a* concentration in subsurface layer and the three parameters of SCM (SCML depth, thickness and intensity) were obtained and discussed.

## 2 Model and Data

### 2.1 1-D Physical-Biochemical Model

In this study, the Modular Ecosystem Model-1D (MEM-1D) is used to simulate the physical and biogeochemical processes in the SCS. The physical sub-model in MEM-1D is part of the Princeton Ocean Model (POM), in which only the vertical sigma coordinate and time are considered as independent variables. The model has 40 layers with varying thicknesses from the surface to 1200 m in the vertical direction. The vertical turbulence mixing is parameterized with a 2.5-level turbulence closure scheme. The time step is 216 s. The initial conditions of temperature and salinity are based on the January observations from the National Center for Ocean Research, Taiwan (http://ncor.odb.ntu.edu.tw/odbs/seats/index.htm). The surface forcing includes the climatological daily mean wind, monthly sea surface temperature and salinity from the NCEP/NCAR reanalysis. The solar radiation is calculated using the SBDART (Santa Barbara DISORT Atmospheric Radiative Transfer) software.

The biochemical sub-model is taken from the European Regional Sea Ecosystem Model (ERSEM III, Fig.2) (Vichi *et al.*, 2004). The model can reproduce the seasonal variations of vertical phytoplankton profiles in the eastern part of the South Yellow Sea (Xia and Gao, 2006) and in the northern SCS (Zhang *et al.*, 2011). However, despite the fact that the <3 μm phytoplankters are the dominant species in the SCML of the SCS (Huang *et al.*, 2002; Lee Chen, 2005; Ning *et al.*, 2004), Zhang *et al.* (2011) only considered diatom in their model, and the modelled chlorophyll concentrations in SCML were significantly lower than the observations. Takahashi and Hori (1984) reported that more than 70% of Chl-*a* concentration in the SCML was derived from picoplankton in the SCS. Therefore, flagellate and picophytoplankton are considered in this study. The biochemical model has six compartments (14 state variables), including nutrient (nitrate, ammo-

nium, phosphate, silicate), phytoplankton (diatom (20–200 μm), flagellate (2–20 μm), picophytoplankton (0.2–2 μm)), zooplankton (omnivorous, heterotrophic nanoflagellates, and microzooplankton), bacteria, organic detritus (dissolved organic detritus and particulate organic detritus), and dissolved oxygen. The dynamics of each biogeochemical state variable ($C_i$), a function of spatial vector and time, is given by a partial differential equation written in the following form:

$$\frac{\partial C_i}{\partial t} = -w_C \frac{\partial C_i}{\partial z} + \frac{\partial}{\partial z}\left( K_z \frac{\partial C_i}{\partial z} \right) + J_i \ (i = 1, 2, \cdots, 14), \quad (1)$$

where $w_C$ is the vertical velocity, $K_z$ is the diffusivity coefficient, and $J_i$ represents the biogeochemical term and equals to the net production.

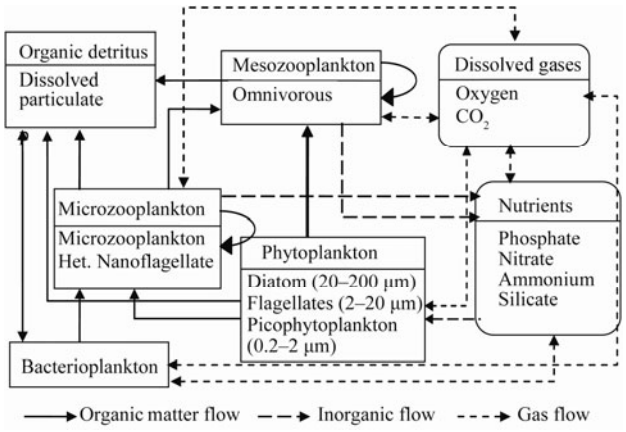


Fig.2 Scheme of the biogeochemical model adapted from Vichi *et al.* (2004).

A variable chlorophyll-to-carbon ratio of phytoplankton is proposed in this model. Consequently, Chl-*a* concentration is also set as a state variable, defined as an additional vector component of phytoplankton in unit of mg m$^{-3}$. The formula of Chl-*a* synthesis is presented in Appendix A.

The PAR is parameterized according to the Lambert-Beer formulation with depth dependent attenuation coefficients (Eq. (A3)). Light propagation takes into account the extinction due to water, phytoplankton, particulate detritus, and suspended inorganic (Eq. (A4)). The parameters used in this model are presented in Appendix B. The maximum growth rate, respiration rate, excretion rate of phytoplankton at 20℃, the sinking velocity of phytoplankton, the background light attenuation, and the other biogeochemical parameters were adapted from previous studies (Lu *et al.*, 2010; Bienfang, 1980; Lee Chen, 2005; Liu *et al.*, 2002; Liu *et al.*, 2007; Vichi *et al.*, 2004).

The initial conditions of nutrient concentration, Chl-*a* concentration, zooplankton, and bacteria were obtained from Marine Atlas of the South China Sea (116˚E, 18˚N). Note that nutrient input from atmosphere or through ocean current is not included. Simulations start from winter and run for three years. The results obtained in the second year are analyzed, which are almost the same as those in the third year.

Model sensitivity experiments were carried out to investigate influencing factors of SCMs by changing model parameters. The sensitivity of a predicted variable to a selected parameter is quantified as:

$$S = \left| \frac{\text{Change of predicted variable}}{\text{Change of parameter}} \right|. \quad (2)$$

### 2.2 Fitting Model

The thickness, depth and intensity of the SCML were selected as indices to characterize the SCMs. They can be derived from a shifted-Gaussian model (Lewis *et al.*, 1983; Platt *et al.*, 1988):

$$P(z) = \frac{h}{\sigma\sqrt{2\pi}} \mathrm{e}^{-\frac{(z-z_m)^2}{2\sigma^2}}, \quad (3)$$

where $P(z)$ (mg m$^{-3}$) is the Chl-*a* concentration as a function of depth $z$ (m), $h$ (mg m$^{-2}$) is the integrated Chl-*a* concentration in water column, $z_m$ (m) is the depth of the Chl-*a* concentration maximum, and $\sigma$ (m) is the width of the peak.

The simulated Chl-*a* concentration is vertically homogeneous in the upper layer, but increases with the depth and then peaks at the subsurface layer. Therefore, the shifted Gaussian function is revised to a piecewise function:

$$P(z) = \begin{cases} P_0 & 0 \le z \le z_s \\ \dfrac{h}{\sigma\sqrt{2\pi}} \mathrm{e}^{-\frac{(z-z_m)^2}{2\sigma^2}} & z_s \le z < z_b \end{cases}, \quad (4)$$

where $z_s$(m) denotes the bottom depth of the upper layer, $P_0$ is the Chl-*a* concentration (mg m$^{-3}$) above $z_s$. $z_b$ is the maximum depth where Chl-*a* concentration can be detected, assumed to be 200 m here. It is noted that the upper layer depth, $z_s$, is time-dependent, and it is shallower (~40 m) in winter and roughly constant (~50 m) in the other seasons.

In this paper, the thickness, the depth, and the intensity of SCML are defined as $2\sigma$, $z_m$, and $\frac{h}{\sigma\sqrt{2\pi}}$, respectively.

### 2.3 Data

Ten datasets at the SEATS station from September 1999 to May 2004, including Chl-*a* concentration, temperature and salinity profiles (Liu *et al.*, 2002; Liu *et al.*, 2007), were used to evaluate the model results. Detailed descriptions of the data can be found in the research by Wong *et al.* (2007a).

## 3. Results

### 3.1 Model Validation

Fig.3 shows the comparison between the observed and calculated vertical profiles of temperature and salinity at the SEATS station in winter (December, January, February),

spring (March, April, May), summer (June, July, August), and fall (September, October, November). The observed vertical profiles are fairly well reproduced by the model results, except for the salinity bias in spring and fall.

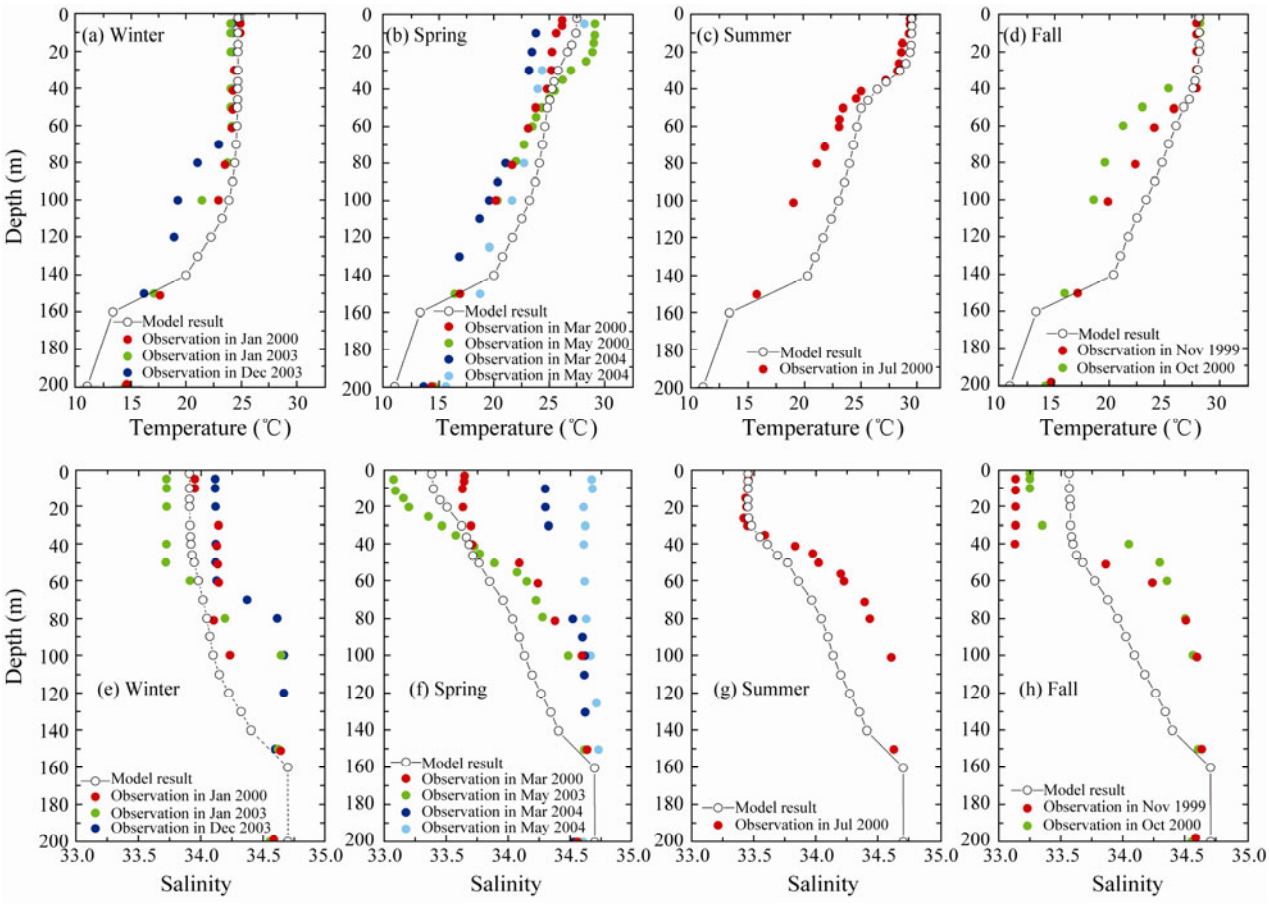


Fig.3 Observed (dots) and modeled (line with circles) vertical profiles of temperature (a, b, c, and d) and salinity (e, f, g, and h) at SEATS station in the SCS in four seasons.

In this study, the mixed layer depth (MLD) is defined as the depth above which there is a temperature drop of 0.5℃ from the sea surface temperature (Karl and Lukas, 1996). The calculated MLD agrees reasonably well with the observed monthly average MLD (Fig.4). Note that the observed MLD was defined as the depth above which the density gradients was $\leq 0.1\sigma_\theta$ unit $m^{-1}$ (Tseng *et al.*, 2005; Wong *et al.*, 2007b). Wong *et al.* (2007b) found that both definitions above yielded similar results. The cruises for the MLD observations are shown in Table 1.

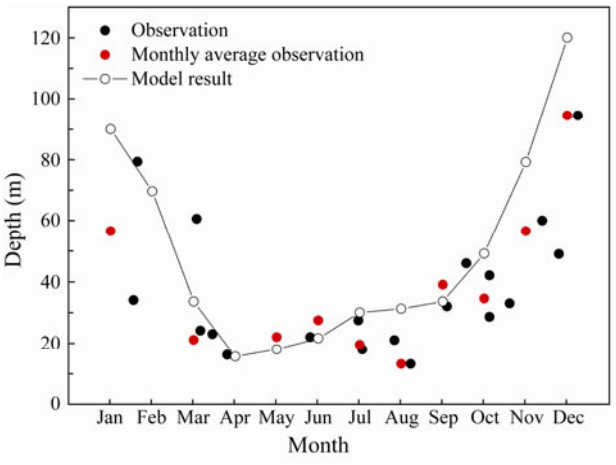


Fig.4 Observed (black dots), observed monthly average (red dots) and calculated (line with circles) mixed layer depth (MLD).

Table 1 Cruises for the MLD observations at the SEATS station in the SCS

| R/V | Cruise | Date |
|---|---|---|
| Ocean Research III | 561 | September 17–22, 1999 |
| | 585 | November 22–26, 1999 |
| | 600 | January 17–18, 2000 |
| | 607 | March 12–17, 2000 |
| | 629 | May 23–26, 2000 |
| | 644 | July 25–27, 2000 |
| | 657 | October 16–21, 2000 |
| | 682 | February 27–March 4, 2001 |
| | 716 | June 27–July 1, 2001 |
| | 729 | October 2–7, 2001 |
| | 794 | July 1–3, 2002 |
| Ocean Research I | 632 | December 5–11, 2001 |
| | 639 | March 19–April 2, 2002 |
| | 656 | September 3–4, 2002 |
| | 664 | November 11–13, 2002 |
| | 673 | January 20–21, 2003 |
| | 674 | March 5–6, 2003 |
| | 690 | August 7–8, 2003 |
| | 696 | October 4–5, 2003 |

The modeled seasonal mean Chl-*a* concentration in the top 200 m matches the observed values at the SEATS station in different seasons (Fig.5). During winter, the combined effect of surface cooling and wind-induced mixing brings nutrients from the upper nutricline into the surface mixed layer to support primary production. As a result, a distinct surface chlorophyll maximum is often found in winter while surface Chl-*a* concentration is low for most of the year. A permanent SCM exists in all seasons except winter in the SCS. However, in January 2000, the observed vertical distribution of Chl-*a* concentration shows an obvious SCM. Therefore, only using the 2000 data for the analysis (Zhang *et al.*, 2011) cannot give a fair assessment of the model performance and more observations are used for the model validation.

Fig.5 also shows that both observed and simulated vertical profiles of Chl-*a* concentration can be well fitted by the piecewise function (Eq. (4)) in all seasons, except for the observations in January and December 2003. The square of the correlation coefficient is greater than 0.9 ($P$<0.05).

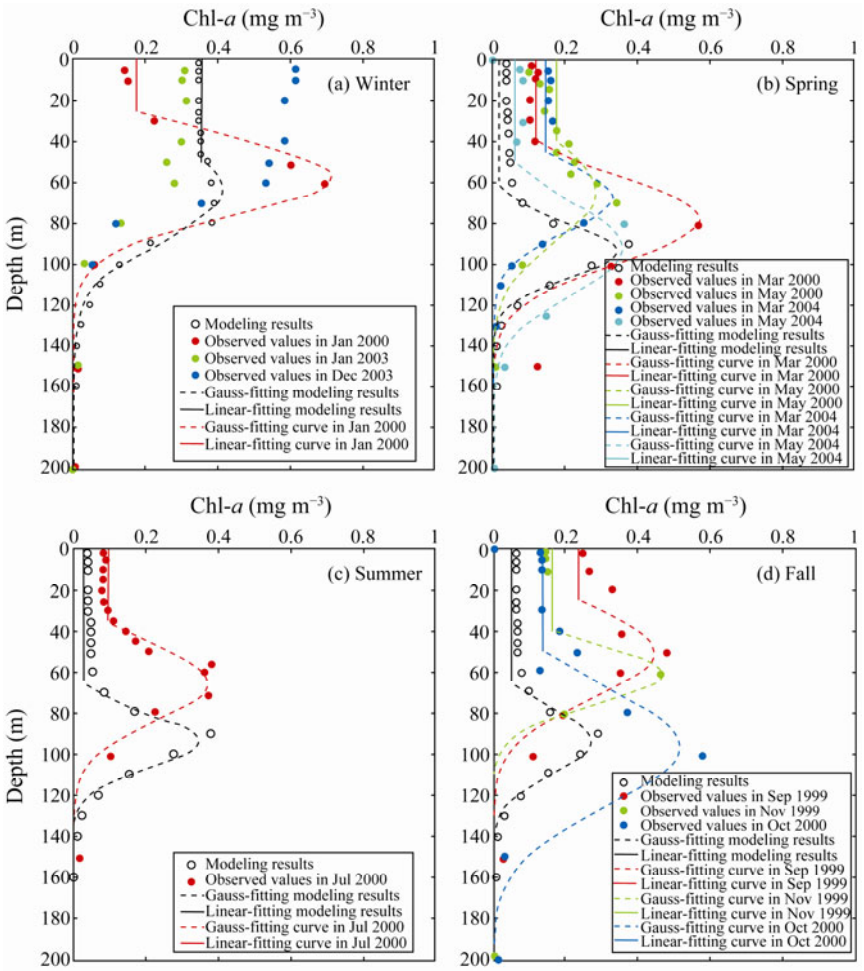


Fig.5 Observed (dots) and simulated (circles) vertical profiles of Chl-*a* concentration in four seasons. Solid and dotted lines are the fitting curves of observations and model results.

### 3.2 Seasonal Variations of SCM Characteristics

The model results show that a SCM occurs in all the months, although it is less significant in winter than in the other seasons. The depth of SCML ($z_m$) typically occurs at 75 m with a range of ±10 m (Fig.6a). Seasonally, the SCML depth is shallower in winter, at a water depth of 50–67 m, and it ranges from 70–85 m in the other seasons. The SCML thickness ($2\sigma$) ranges from 26–47 m, averaging 31±6.7 m (Fig.6b). The SCML intensity ($\frac{h}{\sigma\sqrt{2\pi}}$) exhibits a clear seasonal variation (Fig.6c). The highest and the lowest are 0.66 mg m$^{-3}$ in winter and 0.22 mg m$^{-3}$ in fall, respectively. The annual average SCML intensity is 0.37 ±0.11 mg m$^{-3}$.

## 4 Discussion

### 4.1 Responses to East Asian Monsoon

Measured surface wind speed in the SCS is about 10 m s$^{-1}$ during winter season, and 5 m s$^{-1}$ during summer season. Two numerical experiments were carried out to study the influence of the East Asian Monsoon on SCMs. In the first experiment, Wind_0.5, the winter wind speed was set to equal half of the default value in the practicing model now (CTRL, control run), and in the second one, Wind_2, the summer wind speed equals two times the default value.

The model results show that the SCML depth, thickness, and intensity are varying differently corresponding to different wind speeds in winter and summer (Fig.7 top panel). The depths of SCML vary slightly both in winter

and summer, especially in summer ($S$=0.06, Table 2). These results are consistent with the research done for the shelf of the northern SCS in summer (Lu *et al.*, 2010), in which the depth of SCML hardly shows any change under changing wind stress.

In summer, the stronger wind can entrain more nutrients to the upper layer by deepening the MLD (Fig.7 right bottom). The SCML thickness increases by 46% due to the lifted top boundary of SCML, and its intensity decreases by 30% (Table 2). In winter, the weaker wind leads to a significant thick SCML because a stratified and stable water column is favorable for the formation of SCMs.

Fig.7 also shows that the change of Chl-*a* concentration corresponds to that of nitrate concentration in the euphotic zone. These results suggest that nitrate is a major influential factor on Chl-*a* concentration. Wind-induced mixing mainly affects the SCML thickness and intensity by changing the nitrate transport from the nitrate-rich water to the upper layer.

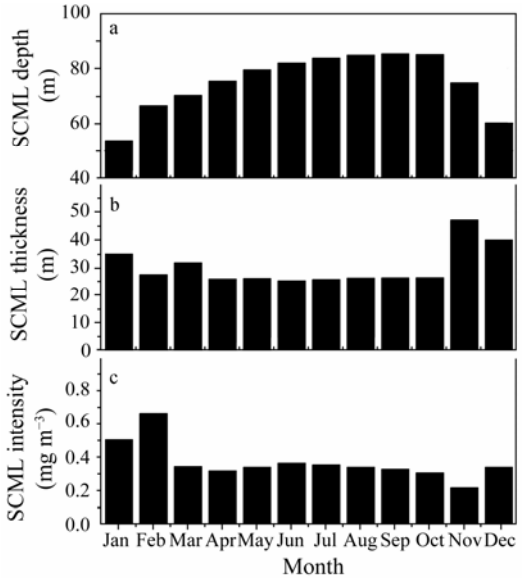


Fig.6 Seasonal variations of modeled SCM characteristics (a) SCML depth, (b) SCML thickness, and (c) SCML intensity.

Table 2 Sensitivity (S) of the simulated SCM characteristics to wind speed, initial nutrient concentration, and light attenuation

| Sensitivity experiment | Winter | | | Spring | | | Summer | | | Fall | | |
|---|---|---|---|---|---|---|---|---|---|---|---|---|
| | Depth | Thickness | Intensity | Depth | Thickness | Intensity | Depth | Thickness | Intensity | Depth | Thickness | Intensity |
| Wind_0.5 | 0.24 | 0.40 | 0.36 | / | / | / | / | / | / | / | / | / |
| Wind_2 | / | / | / | / | / | / | 0.06 | 0.46 | 0.30 | / | / | / |
| Nutrient_0.5 | 0.06 | 0.14 | 0.88 | 0.06 | 0.18 | 0.64 | 0.04 | 0.22 | 0.80 | 0.04 | 0.14 | 0.79 |
| Nutrient_2 | 0.16 | 0.22 | 0.86 | 0.11 | 0.17 | 0.86 | 0.10 | 0.02 | 0.23 | 0.11 | 0.10 | 0.36 |
| Light_0.8 | 0.85 | 2.05 | 1.05 | 0.95 | 1.05 | 0.80 | 0.90 | 1.30 | 0.95 | 1.05 | 0.60 | 1.25 |
| Light_1.2 | 0.70 | 0.85 | 0.40 | 0.50 | 1.60 | 0.95 | 0.60 | 0.30 | 0.65 | 0.65 | 0.55 | 0.30 |

Note: / not analyzed.

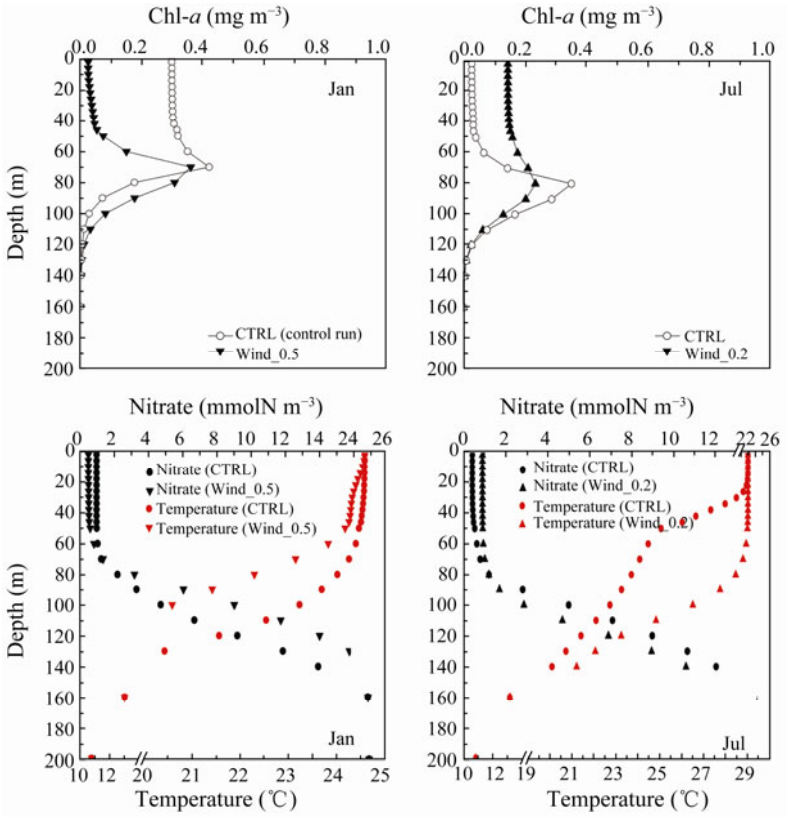


Fig.7 Vertical profiles of Chl-*a* concentration, nitrate concentration and temperature in winter (left panels) and summer (right panels) under different wind speeds.

### 4.2 Responses to the Initial Nutrient Concentration

There are two important processes influencing nutrient concentrations within the surface layer in the SCS during winter. The northeast monsoon forces a cyclonic gyre over the entire basin of the SCS (Shaw and Chao, 1994), which induces a strong upwelling and moves more nutrients up to the surface layer (Ning *et al.*, 2004). The other process is the mineral dust and atmospheric nitrogen deposition into the SCS due to monsoon (Lin *et al.*, 2007; Merrill *et al.*, 1989). Different nutrient levels may change the vertical distribution of Chl-*a* concentration. Two numerical experiments, Nutrient_2 and Nutrient_0.5, were designed for sensitivity tests of the SCM characteristics under different nutrient concentrations. The initial nutrient concentrations for the experiments are set to two times and half of the default value, respectively.

Model results indicate that increasing initial nutrient concentration leads to higher nutrient level through the year (Fig.8). The growth of phytoplankton is limited more by nitrate than by phosphate in the SCS (Chen *et al.*, 2004; Lee Chen, 2005). As initial nutrient concentration increases, nitrate is rapidly consumed by the growth of phytoplankton in the upper layer and the nutrient concentration remains low (Fig.8).

High nutrient level in water column leads to a signify-

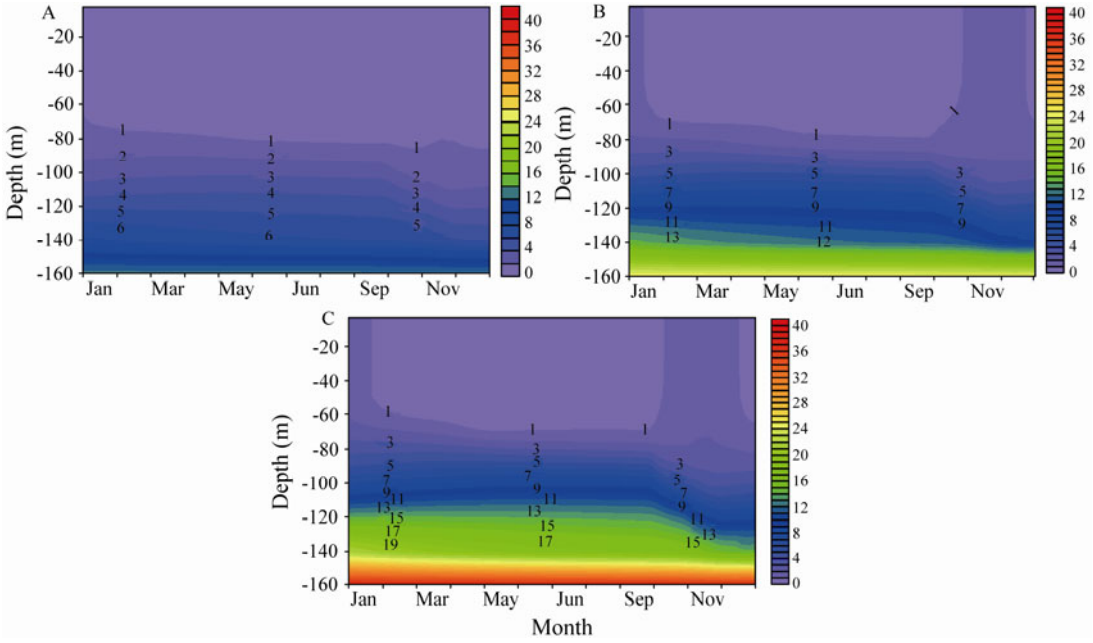


Fig.8 Seasonal variations of nitrate concentrations under (A) half of initial nutrient concentrations, (B) default values, and (C) two times initial nutrient concentrations.

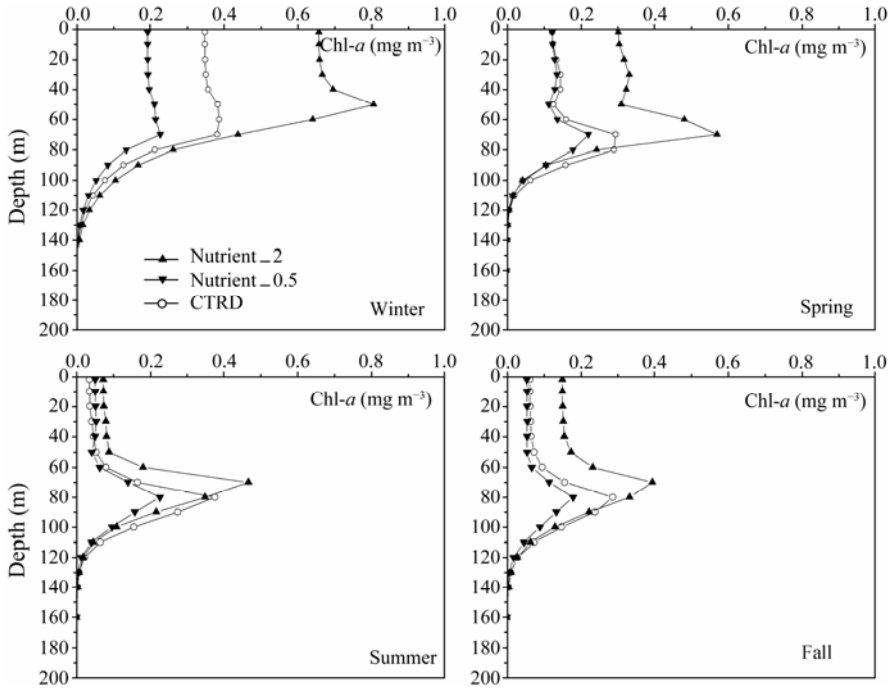


Fig.9 Simulated vertical distributions of Chl-*a* concentration with different initial nutrient concentrations.

cant increase in chlorophyll concentration in the euphotic zone through the whole year, particularly in winter and spring (Fig.9). Doubling initial nutrient concentrations increases the SCML intensity significantly, and vice versa ($0.23<S<0.88$) (Table 2). In winter and spring, the intensity is 80% bigger than that of control run (Table 2). However, the SCML depth and thickness do not show obvious variations ($0.04<S<0.22$) under higher or lower nutrient levels (Table 2). Mellard *et al.* (2011) found that the nutrient input from sediments to the mixed layer enhances light limitation and brings phytoplankton towards the surface, while the SCML intensity increases and remains unaffected. Therefore it can be concluded that nutrient enrichment in water column decreases the SCML depth and thickness, and significantly strengthens the intensity.

### 4.3 Responses to Light Attenuation

The light attenuation is critical in determining the SCML depth in oligotrophic ocean (Varela *et al.*, 1994). It is commonly assumed that the light attenuation can be decomposed and expressed with a set of partial attenuation coefficients, such as the attenuation by water, phytoplankton, and suspended particulate matter. Compared with the background light attenuation, variations of shelf shading by organic materials (both phytoplankton and detritus) have a minor effect on SCM characteristics in oligotrophic ocean (Beckmann and Hense, 2007). In order to estimate the variations of SCM characteristics responding to light in the SCS, the background light attenuation coefficient is set to 20% more and less than that in the control run (Light_0.8 and Light_1.2 in Table 2), respectively.

The model results show that the background light attenuation has a profound effect on the three parameters of SCM (Fig.10). In winter, the better penetration of light makes phytoplankton migrating downwards out of the upper mixed layer, leading to a more obvious SCM. In the other seasons, the 20% weakening of light attenuation and the increased nutrient availability in deeper water induce the 20% deepening and thickening of SCML ($S$~1.00, Table 2), and the over 16% increase in intensity ($0.80<S<1.25$).

Fig.11 shows that the nutricline depth shoals with a high light attenuation coefficient. Increased light attenuation decreases the light availability in water column. Thus, phytoplankton tends tomove upward to sustain growth, resulting in a shallower nutricline. This result is consistent with the research findings by Klausmeier and Litchman (2001), in which it was shown that the SCML depth determines the location of nutricline, and not vice versa.

## 5 Conclusions

A 1-D coupled physical-biological model is used to examine the seasonal variations of SCMs in the SCS, and their responses to changes of the northeast monsoon, initial nutrient level and background light attenuation. The SCMs are quantified by the SCML depth, thickness, and intensity, which are obtained from fitting the vertical profiles of Chl-*a* concentration by a Gaussian function. Driven by climatological forcing, the model results well reproduce the observed SCMs. The modeling study is able to identify the key characteristics and processes of the SCMs at the SEATS station in the SCS.

A strong SCM exists through the year except in December. During the northeast monsoon, as the SCML is situated closer to the surface, a thick SCML together with a high intensity occurs.

The strength of monsoon is the main influential factor for the formation of SCMs. Due to the strong vertical mixing under the northeast monsoon, the SCML intensity tends to be diminished. However, high wind-induced vertical mixing has effect on the SCML thickness and intensity, but almost no effect on the SCML depth in summer.

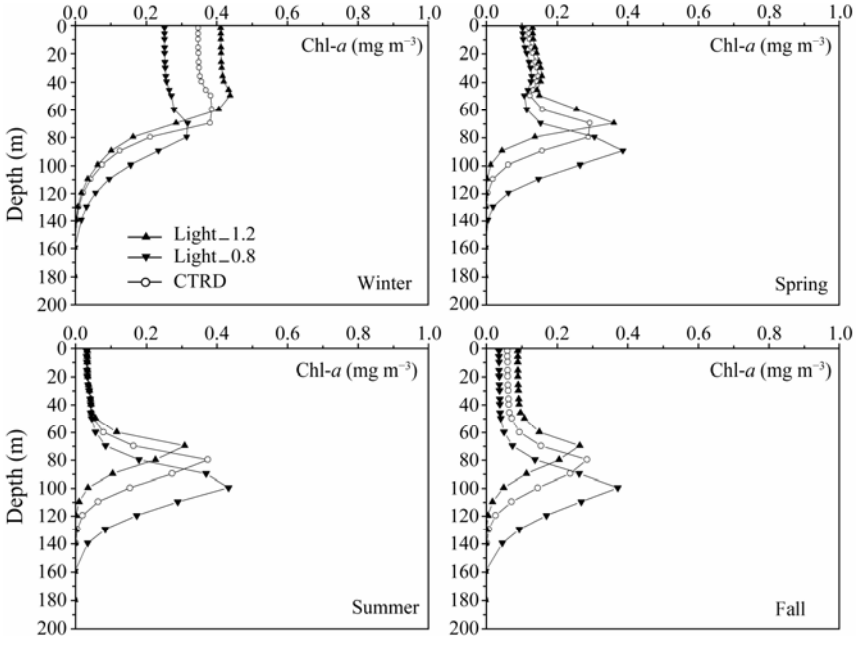


Fig.10 Simulated vertical distributions of Chl-*a* concentration under different background light attenuation.

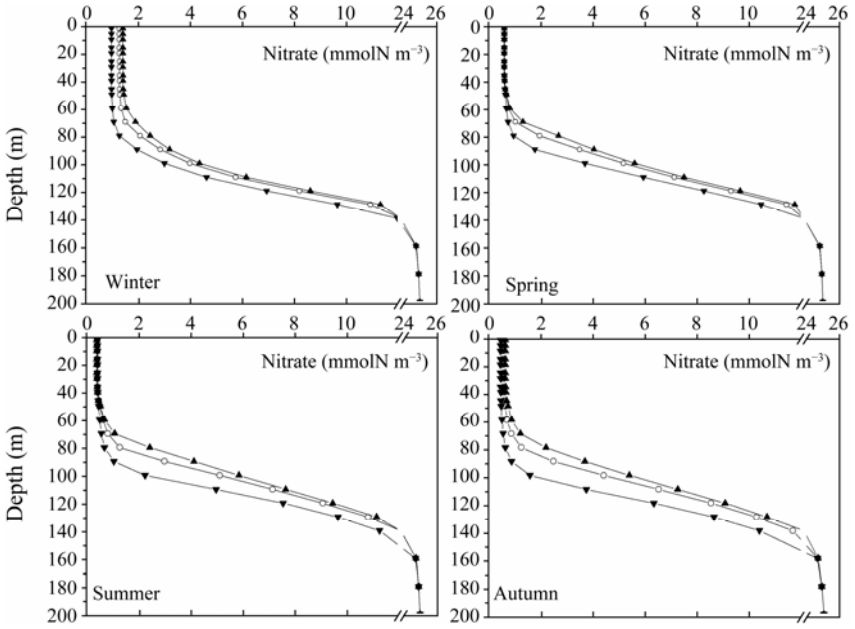


Fig.11 The same as Fig.10 except for nitrate concentration.

Besides the profound influence on the SCML intensity by initial nutrient level, the light attenuation is crucial to the SCM characteristics, especially for the SCML depth and thickness. Both the nutrient enrichment in water column and background light attenuation positively influence the SCML intensity and will lead to a thinner and shallower SCML.

In short, the depth and thickness of SCML are mainly controlled by light attenuation, and the SCML thickness is partly influenced by wind. The SCML intensity is determined by wind, light attenuation and initial nitrate concentration in the SCS.

## Acknowledgements

This work was supported by the National Natural Science Foundation of China (Nos. 41106007, 41210008), the China Postdoctoral Science Foundation (No. 2013M 541958), and the International Cooperation Project of China (No. 2010DFA91350).

## Appendix A

Chl-*a* concentration is calculated by:

$$Chla = \sum_{m=1}^{3} P_l^{(m)} , \quad (A1)$$

where $P_l$ is the chlorophyll-content in phytoplankton. The time variation of $P_l$ is given by:

$$\frac{dP_l}{dt} = \rho_{chl} g_P P_c + d_{0_P} P_l , \rho_{chl} = \rho_{chl}^0 f_P^n \frac{r_P}{\frac{P_i}{P_c}\alpha_{chl} I_{PAR}} , \quad (A2)$$

where $P_c$ is the carbon component of phytoplankton, $g_P$ is the net carbon uptake, and $d_{0_P}$ is the maximum specific growth rate. The parameter $\rho_{chl}$ is the ratio between the energy assimilated and the energy absorbed, where $\rho_{chl}^0$ is the maximum Chl-*a*: C quotum, $f_P^n$ is the regulating factor for the nitrate limitation, $r_P$ is the photosynthetic gross rate, and $\alpha_{chl}$ is the initial slope of the P-I curve.

The parameter $I_{PAR}$ represents the PAR:

$$I_{PAR} = \varepsilon_{PAR} Q_s \exp(\lambda_w z + \int_z^0 \lambda_{bio}(z')dz') , \quad (A3)$$

where $\varepsilon_{PAR}$ is the coefficient to determine the portion of PAR (usually 0.5), $Q_S$ is the surface short-wave irradiance flux, $\lambda_w$ is the background extinction of water, and

$$\lambda_{bio} = \sum_j \underset{(1)}{c_{P(j)} P_i^{(j)}} + \underset{(2)}{c_{R^{(6)}} R_c^{(6)}} + \underset{(3)}{c_{ISM}\, ISM} \quad (A4)$$

is the extinction due to the three terms on the right hand side of Equation (A4): phytoplankton (1), particulate detritus (2), and inorganic suspended matter (3).

## Appendix B

Biogeochemical sub-model parameters

Table B1 Optical parameters

| Description | Unit | Value | Reference |
|---|---|---|---|
| Extinction coefficient: diatoms | $m^{-1}\,mg\,C^{-1}$ | $0.5\times10^{-3}$ | Vichi *et al.*, 2004 |
| Extinction coefficient: flagellates | $m^{-1}\,mg\,C^{-1}$ | $0.4\times10^{-3}$ | Vichi *et al.*, 2004 |
| Extinction coefficient: picoplankton | $m^{-1}\,mg\,C^{-1}$ | $0.4\times10^{-3}$ | Vichi *et al.*, 2004 |
| Extinction coefficient: particulate organic matter | $m^{-1}\,mg\,C^{-1}$ | $0.1\times10^{-3}$ | Vichi *et al.*, 2004 |
| Extinction coefficient: sediment | $m^{-1}\,mg^{-1}$ | $0.04\times10^{-3}$ | Vichi *et al.*, 2004 |
| Background light extinction | $m^{-1}$ | 0.05 | Chen *et al.*, 2004; Lee Chen, 2005 |

Table B2 Phytoplankton parameters

| Description | Unit | Value | | | Reference |
|---|---|---|---|---|---|
| | | Diatom | Flagellate | Picoplankton | |
| Q10 value | – | 2.0 | 2.0 | 2.0 | Vichi *et al.*, 2004 |
| Maximum phytoplankton growth rate at 20℃ | $d^{-1}$ | 2.1 | 2.1 | 2.1 | Liu *et al.*, 2002, 2007 |
| Phytoplankton respiration rate at 20℃ | $d^{-1}$ | 0.15 | 0.1 | 0.1 | Liu *et al.*, 2002, 2007; Vichi *et al.*, 2004 |
| Phytoplankton excretion rate | – | 0.05 | 0.2 | 0.2 | Liu *et al.*, 2002, 2007 |
| Specific affinity constant for N-NO3 | $(mg\,C)^{-1}\,d^{-1}$ | 0.0025 | 0.0025 | 0.0025 | Vichi *et al.*, 2004 |
| Specific affinity constant for N-NH4 | $(mg\,C)^{-1}\,d^{-1}$ | 0.0025 | 0.01 | 0.02 | Vichi *et al.*, 2004 |
| Specific affinity constant for $PO_3$ | $(mg\,C)^{-1}\,d^{-1}$ | 0.0025 | 0.0025 | 0.0025 | Vichi *et al.*, 2004 |
| Sinking velocity | $m\,d^{-1}$ | 1 | 0.5 | 0.1 | Bienfang, 1980; Lu *et al.*, 2010 |
| Minimal dissolution rate | $d^{-1}$ | 0.05 | 0.05 | 0.05 | Vichi *et al.*, 2004 |
| Si Half-saturation constant | $mmol\,Si\,m^{-3}$ | 0.3 | – | – | Vichi *et al.*, 2004 |
| Standard Si:C ratio in diatoms | mmol Si/mg C | 0.03 | – | – | Vichi *et al.*, 2004 |
| C:Chl ratio | mg C/mgChl-*a* | 25.0 | 50.0 | 50.0 | Vichi *et al.*, 2004 |
| Minimal N:C ratio | mmol N/mg C | $0.678\times10^{-2}$ | $0.678\times10^{-2}$ | $0.678\times10^{-2}$ | Vichi *et al.*, 2004 |
| Maximum N:C ratio | mmol N/mg C | 0.0252 | 0.0252 | 0.0252 | Vichi *et al.*, 2004 |
| Minimal P:C ratio | mmol P/mg C | $0.428\times10^{-3}$ | $0.428\times10^{-3}$ | $0.428\times10^{-3}$ | Vichi *et al.*, 2004 |
| Maximum P:C ratio | mmol P/mg C | $0.157\times10^{-2}$ | $0.157\times10^{-2}$ | $0.157\times10^{-2}$ | Vichi *et al.*, 2004 |

Table B3 Zooplankton parameters (Vichi *et al.*, 2004)

| Description | Unit | Value | | |
|---|---|---|---|---|
| | | Heterotrophic flagellates | Microzoo-plankton | Mesozoo-plankton |
| Maximum growth rate | $d^{-1}$ | 5.0 | 1.2 | 0.5 |
| Assimilation efficiency | – | 0.4 | 0.5 | 0.5 |
| Basal respiration rate | $d^{-1}$ | 0.02 | 0.02 | 0.02 |
| Fraction of excretion going to DOM | – | 0.5 | 0.5 | 0.5 |
| Mortality rate | $d^{-1}$ | 0.25 | 0.25 | 0.2 |

Table B4 Bacterial and detrital parameters (Vichi *et al.*, 2004)

| Description | Units | Value |
|---|---|---|
| Assimilation rate | $d^{-1}$ | 8.38 |
| Basal respiration rate | $d^{-1}$ | 0.02 |
| Mortality rate | $d^{-1}$ | 0.05 |
| Q10 value for bacterial | – | 2.95 |
| Dissolution of dissolved organics to inorganics | $d^{-1}$ | 0.05 |
| Fraction of detritus break down | $d^{-1}$ | 0.01 |
| Relative nitrification rate | $d^{-1}$ | 0.05 |

## References


Beckmann, A., and Hense, I., 2007. Beneath the surface: Characteristics of oceanic ecosystems under weak mixing conditions-A theoretical investigation. *Progress in Oceanography*, **75** (4): 771-796.

Bienfang, P. K., 1980. Phytoplankton sinking rates in oligotrophic waters off Hawaii, USA. *Marine Biology*, **61** (1): 69-77.

Chen, C. C., Shiah, F. K., Chung, S. W., and Liu, K. K., 2006. Winter phytoplankton blooms in the shallow mixed layer of the South China Sea enhanced by upwelling. *Journal of Marine Systems*, **59** (1): 97-110.

Chen, Y. L., Chen, H. Y., Karl, D. M., and Takahashi, M., 2004. Nitrogen modulates phytoplankton growth in spring in the South China Sea. *Continental Shelf Research*, **24** (4-5): 527-541.

Cullen, J. J., 1982. The deep chlorophyll maximum: Comparing vertical profiles of chlorophyll *a*. *Canadian Journal of Fisheries and Aquatic Sciences*, **39** (5): 791-803.

Fennel, K., and Boss, E., 2003. Subsurface maxima of phytoplankton and chlorophyll: Steady-state solutions from a simple model. *Limnology and Oceanogoraphy*, **48** (4): 1521-1534.

Gong, X., Shi, J., and Gao, H. W., 2012. Subsurface chlorophyll maximum in ocean: Its characteristics and influencing factors. *Advances in Earth Science*, **27** (5): 539-548.

Hanson, C. E., Pesant, S., Waite, A. M., and Pattiaratchi, C. B., 2007. Assessing the magnitude and significance of deep chlorophyll maxima of the coastal eastern Indian Ocean. *Deep-Sea Research Part II*, **54** (8-10): 884-901.

Hense, I., and Beckmann, A., 2008. Revisiting subsurface chlorophyll and phytoplankton distributions. *Deep Sea Research Part I*, **55** (9): 1193-1199.

Hodges, B. A., and Rudnick, D. L., 2004. Simple models of steady deep maxima in chlorophyll and biomass. *Deep-Sea Res Part I*, **51** (8): 999-1015.

Holm-Hansen, O., and Hewes, C. D., 2004. Deep chlorophyll-*a* maxima (DCMs) in Antarctic waters. *Polar Biology*, **27** (11): 699-710.

Hopkinson, B. M., and Barbeau, K. A., 2008. Interactive influences of iron and light limitation on phytoplankton at subsurface chlorophyll maxima in the eastern North Pacific. *Limnology and Oceanography*, **53** (4): 1303-1318.

Huang, B. Q., Lin, X. J., Liu, Y., Dai, M. H., Hong, H. S., and Williams, K. K. L., 2002. Ecological study of picoplankton in northern South China Sea. *Chinese Journal of Oceanology and Limnology*, **20** (Special Issue): 22-32.

Huisman, J., Thi, N., Karl, D. M., and Sommeijer, B., 2006. Reduced mixing generates oscillations and chaos in the oceanic deep chlorophyll maximum. *Nature*, **439** (7074): 322-325.

Jamart, B. M., Winter, D. F., Banse, K., Anderson, G. C., and Lam, R. K., 1977. A theoretical study of phytoplankton

growth and nutrient distribution in the Pacific Ocean off the northwestern US coast. *Deep-Sea Research*, **24** (8): 753-773.

Karl, D. M., and Lukas, R., 1996. The Hawaii Ocean Time-series (HOT) program: Background, rationale and field implementation. *Deep-Sea Research Part II*, **43** (2): 129-156.

Klausmeier, C. A., and Litchman, E., 2001. Algal games: The vertical distribution of phytoplankton in poorly mixed water columns. *Limnology and Oceanography*, **8** (46): 1998-2007.

Lee Chen, Y., 2005. Spatial and seasonal variations of nitrate-based new production and primary production in the South China Sea. *Deep-Sea Research Part I*, **52** (2): 319-340.

Lewis, M. R., Cullen, J. J., and Platt, T., 1983. Phytoplankton and thermal structure in the upper ocean: consequences of nonuniformity in chlorophyll profile. *Journal of Geophysical Research*, **88** (C4): 2565-2570.

Lin, I. I., Chen, J. P., Wong, G. T. F., Huang, C. W., and Lien, C. C., 2007. Aerosol input to the South China Sea: Results from the MODerate resolution imaging spectro-radiometer, the quick scatterometer, and the measurements of pollution in the troposphere sensor. *Deep-Sea Research Part II*, **54** (14-15): 1589-1601.

Liu, K. K., Chao, S. Y., Shaw, P. T., Gong, G. C., Chen, C. C., and Tang, T. Y., 2002. Monsoon-forced chlorophyll distribution and primary production in the South China Sea: Observations and a numerical study. *Deep-Sea Research Part I*, **49** (8): 1387-1412.

Liu, K. K., Chen, Y. J., Tseng, C. M., Lin, I. I., Liu, H. B., and Snidvongs, A., 2007. The significance of phytoplankton photo-adaptation and benthic-pelagic coupling to primary production in the South China Sea: Observations and numerical investigations. *Deep-Sea Research Part II*, **54** (14-15): 1546-1574.

Lu, Z., Gan, J., Dai, M., and Cheung, A., 2010. The influence of coastal upwelling and a river plume on the subsurface chlorophyll maximum over the shelf of the northeastern South China Sea. *Journal of Marine Systems*, **82** (1-2): 35-46.

Martin, J., Tremblay, J., Gagnon, J., Tremblay, G., Lapoussière, A., Jose, C., Poulin, M., Gosselin, M., Gratton, Y., and Michel, C., 2010. Prevalence, structure and properties of subsurface chlorophyll maxima in Canadian Arctic waters. *Marine Ecology Progress Series*, **412**: 69-84.

Mellard, J. P., Yoshiyama, K., Litchman, E., and Klausmeier, C. A., 2011. The vertical distribution of phytoplankton in stratified water columns. *Journal of Theoretical Biology*, **269** (1): 16-30.

Merrill, J. T., Uematsu, M., and Bleck, R., 1989. Meteorological analysis of long range transport of mineral aerosols over the North Pacific. *Journal of Geophysical Research*, **94** (D6): 8584-8598.

Ning, X., Chai, F., Xue, H., Cai, Y., Liu, C., and Shi, J., 2004. Physical-biological oceanographic coupling influencing phytoplankton and primary production in the South China Sea, *Journal of Geophysical Research*, **109**: 1-20.

Pérez, V., Fernández, E., Mara Ón, E., Morán, X., and Zubkov, M. V., 2006. Vertical distribution of phytoplankton biomass, production and growth in the Atlantic subtropical gyres. *Deep-Sea Research Part I*, **53** (10): 1616-1634.

Platt, T., Sathyendranath, S., Caverhill, C. M., and Lewis, M. R., 1988. Ocean primary production and available light: Further algorithms for remote sensing. *Deep-Sea Research Part I*, **35** (6): 855-879.

Radenac, M. H., and Rodier, M., 1996. Nitrate and chlorophyll distributions in relation to thermohaline and current structures in the western tropical Pacific during 1985–1989. *Deep-Sea Research Part II*, **43** (4-6): 725-752.

Riley, G. A., Stommel, H., and Bumpus, D. F., 1949. Quantitative ecology of the plankton of the western North Atlantic. *Bulletin Bingham Oceanographical Collection*, **12** (3): 1-69.

Shaw, P. T., and Chao, S. Y., 1994. Surface circulation in the South China Sea. *Deep-Sea Research Part I*, **41** (11-12): 1663-1683.

Shaw, P. T., Chao, S. Y., Liu, K. K., Pai, S. C., and Liu, C. T., 1996. Winter upwelling off Luzon in the northeastern South China Sea. *Journal of Geophysical Research*, **101** (16): 416-435.

Siswanto, E., Ishizaka, J., and Yokouchi, K., 2005. Estimating Chlorophyll-*a* vertical profiles from satellite data and the implication for primary production in the Kuroshio front of the East China Sea. *Journal of Oceanography*, **61** (3): 575-589.

Takahashi, M., and Hori, T., 1984. Abundance of picophytoplankton in the subsurface chlorophyll maximum layer in subtropical and tropical waters. *Marine Biology*, **79** (2): 177-186.

Tang, D. L., Ni, I. H., Kester, D. R., and Muller-Karger, F. E., 1999. Remote sensing observations of winter phytoplankton blooms southwest of the Luzon Strait in the South China Sea. *Marine Ecology–Progress Series*, **191**: 43.

Teira, E., Mourio, B., Mara ón, E., Pérez, V., Pazo, M. J., Serret, P., de Armas, D., Escanez, J., Woodward, E., and Fernández, E., 2005. Variability of chlorophyll and primary production in the Eastern North Atlantic Subtropical Gyre: Potential factors affecting phytoplankton activity. *Deep-Sea Research Part I*, **52** (4): 569-588.

Tseng, C. M., Wong, G. T. F., Lin, I. I., Wu, C. R., and Liu, K. K., 2005. A unique seasonal pattern in phytoplankton biomass in low-latitude waters in the South China Sea. *Geophysical Research Letters*, **32** (8), L8608.

Varela, R. A., Cruzado, A., and Tintoré, J., 1994. A simulation analysis of various biological and physical factors influencing the deep-chlorophyll maximum structure in oligotrophic areas. *Journal of Marine Systems*, **5** (2): 143-157.

Venrick, E. L., 1993. Phytoplankton seasonality in the central North Pacific: The endless summer reconsidered. *Limnology and Oceanography*, **38** (6): 1135-1149.

Vichi, M., Baretta, J. W., Baretta-Bekker, J. G., and Al, E., 2004. European Regional Seas Ecosystem Model III: Review of the biogeochemical equations. http://www.bo.ingv.it/ersem3.

Wang, D. X., Du Y., and Shi P., 2002. *Climatological Atlas of Physical Oceanography in the Upper Layer of the South China Sea.* China Meteorological Press, Beijing, 19-42.

Weston, K., Fernand, L., Mills, D. K., Delahunty, R., and Brown, J., 2005. Primary production in the deep chlorophyll maximum of the central North Sea. *Journal of Plankton Research*, **27** (9): 909-922.

Wong, G. T. F., Ku, T. L., Mulholland, M., Tseng, C. M., and Wang, D. P., 2007a. The Southeast Asian time-series study (SEATS) and the biogeochemistry of the South China Sea–an overview. *Deep-Sea Research Part II*, **54** (14-15): 1434-1447.

Wong, G. T. F., Tseng, C. M., Wen, L. S., and Chung, S. W., 2007b. Nutrient dynamics and N-anomaly at the SEATS station. *Deep-Sea Research Part II*, **54** (14-15): 1528-1545.

Xia, J., and Gao, H. W., 2006. Simulation on seasonal cycle vertical structure of plankton ecosystem in eastern area of South Yellow Sea. *Journal of Safety and Environment*, **6** (4): 59-65.

Zhang, C., Shi, J., Gao, H. W., and Gao, Z. H., 2011. Simulation of seasonal cycle of the plankton ecosystem's vertical structure in the northern area (SEATS) of the South China Sea. *Periodical of Ocean University of China*, **41** (3): 11-18.

**(Edited by Xie Jun)**